Quaternary Science Reviews
March 2021, Volume 256 Pages 106839 (14p.)
https://doi.org/10.1016/j.quascirev.2021.106839
https://archimer.ifremer.fr/doc/00680/79190/

Indonesian Throughflow variability over the last two glacial-interglacial cycles: Evidence from the eastern Indian Ocean

Pang Xiaolei [1, 2, *], Bassinot Franck [1], Sepulcre Sophie [2]

[1] Laboratoire des Sciences du Climat et de l'Environnement, LSCE/IPSL, CEA-CNRS-UVSQ, Université Paris-Saclay, Gif-sur-Yvette, 91191, France
[2] Université Paris-Saclay, CNRS, GEOPS, Orsay, 91405, France

* Corresponding author : Xiaolei Pang, email address : xiaolei.pang@outlook.com

Abstract :

We present a Pulleniatina obliquiloculata Mg/Ca-derived thermocline water temperature record (TWT) covering the last 270,000 years at the south of the Lombok Strait, one of the main exits of the Indonesian Throughflow (ITF) into the Indian Ocean. The comparison with TWT records from the Java-Sumatra upwelling system and the Timor Sea suggests that changes in Lombok TWT reflect the balance between the wind-driven Java upwelling and the ITF thermocline transport. We show that the evolution of the TWT gradient (ΔTWT) between the upwelling site and the Lombok site can be used to decipher the relative strength of ITF through time. The 270 ka-long, ΔTWT record shows (i) that the ITF was weaker during MIS 6 and MIS 2–4 compared to the late Holocene, and was enhanced during MIS8, MIS 7, MIS 5 and the early Holocene, and that (ii) it varied with a strong precession-related component. Glacial-interglacial changes may reflect the modulation of ITF by sea-level changes through the modification of ITF pathways in the Indonesian Archipelago, and/or result from changes in the intensity of the Global Conveyor Belt. The strong precession contribution in the relative TWT strength at our Lombok site is interpreted as revealing the importance of southeast monsoon winds on ITF intensity.

Highlights

► We present 270-ka long Mg/Ca derived TWT record in east Indian Ocean. ► The evolution of TWT reflect balance between upwelling and ITF. ► The ITF varied with a strong precession-related component induced by local SE winds. ► The glacial-interglacial ITF change may link to the Global Conveyor Belt variations.

Keywords : Indonesian throughflow, Java upwelling, Mg/Ca temperatures, Indian ocean, Late pleistocene

1. Introduction

The Indonesian Throughflow (ITF) is a complex ocean current system connecting the tropical Pacific and Indian oceans (Gordon, 2005). Every second, ~ 15 million m^3 of water is transported into the Indian Ocean by the ITF. This transport mainly takes place through three principal exits: the Lombok Strait, the Ombai Strait, and the Timor Sea passage (Fig. 1; Sprintall et al., 2009). Modern observations show that ITF transport extends from the surface down to intermediate water depths with maximum transport occurring in the thermocline (Sprintall et al., 2009). The change in ITF salinity, temperature and flux can influence the heat and salinity distribution in the Pacific and Indian Ocean (Hu et al., 2019; Lee et al., 2015). ITF is also a key contributor to the global thermohaline circulation (Gordon, 2005; Talley, 2013). Once in the Indian Ocean, a portion of the ITF water continues its journey as part of the global thermohaline circulation return branch, traveling through the tropical Indian Ocean and being advected within the water masses that leak into the southern Atlantic Ocean as part of the Agulhas current system (Beal et al., 2011). Thus, reconstructing past variability of ITF is mandatory if one wants to fully understand the ocean's role in modulating regional and global climate changes through the redistribution of ocean heat and salinity and the influence of low-latitude processes on high-latitude climate changes.

Over the recent years, oceanographers have gained a better understanding of modern ITF dynamics and hydrographic variability, and their links to low-altitude atmospheric circulation at both seasonal (i.e. Australian-Indonesian monsoon) and inter-annual (i.e. El Niño-Southern Oscillation, ENSO; Indian Ocean Dipole, IOD) timescales (Sprintall et al., 2009; Sprintall and Révelard, 2014). Much less is known, however, regarding ITF variability at longer, centennial to orbital, timescales. On these long timescales, ITF variability is poorly known due to the difficulty of constraining the strength of the ITF, and the paucity of good-quality sedimentary records allowing the reconstruction of hydrographic properties of water masses entering the Indian Ocean. There is no direct way of estimating past changes in the flux of the ITF from sedimentary records. Since the ITF is a heat carrier, it was inferred that past changes in its intensity have impacted the water temperature distribution along its route. Thus, several studies addressed past ITF evolution through the reconstruction of paleo-temperatures at surface and thermocline depths (Fan et al., 2018; Holbourn et al., 2011; Linsley et al., 2010; Xu et al., 2008). However, surface temperatures can prove difficult to interpret in terms of ITF changes owing to the direct impact of radiative forcing (Fan et al., 2018; Holbourn et al., 2011; Linsley et al., 2010; Xu et al., 2008). Changes in thermocline

water temperature (TWT) gradients along the ITF pathway, on the other hand, can be interpreted as reflecting chiefly past changes in ITF dynamics (Fan et al., 2018; Holbourn et al., 2011). Over the last 30 ka, for instance, Fan et al. (2018) showed that the TWT gradient between the north (upstream ITF) and south (downstream ITF) of Makassar Strait (Fig. 1) reached maximum values during the 27-24.2 ka and 19-13.4 ka time intervals. The authors interpreted these two episodes of high TWT gradient as resulting from low thermocline ITF flux which could not maintain a similar TWT between upstream and downstream sites along the ITF. On a longer timescale, over the last 140 ka, Holbourn et al. (2011) had previously found five periods of high East-West TWT gradient in the Timor Sea during marine isotope stage (MIS) 2-4, MIS5b and MIS5d. They interpreted these high TWT gradients as periods of weakened thermocline ITF transport (Holbourn et al., 2011).

The approach based on reconstructing paleo-TWT gradient has provided very important insights about past ITF variability. Yet, some potential drawbacks and puzzling issues remain, which call for further studies. First of all, it is our contention that an ITF proxy based on the reconstruction of paleo-TWT gradients along the main ITF track would lack sensitivity during periods of high ITF fluxes. Once lateral advection is strong enough to result in nearly similar TWT at two sites located apart along the ITF path, an additional increase of ITF flux would not be detected in the temperature gradient. Such a lack of sensitivity may possibly explain why the TWT gradient approach suggests that ITF remained strong and nearly invariant most of the time over the late Quaternary (i.e. null TWT gradient) and collapsed (i.e. non-null TWT gradient) only over a few cold intervals (e.g. MIS2, MIS4, MIS5b and MIS5d; Holbourn et al., 2011; Fan et al., 2018).

Another puzzling element is the unclear relationship between ITF variability and local monsoon wind forcing in the outflow region of Indian Ocean on orbital timescales. Modern oceanographic observations indicate that water transport through the three main ITF exits (i.e., Lombok Strait, Ombai Strait, and Timor Passage) is strongly modulated by seasonal changes in monsoon wind forcing, with increased ITF transport at both surface and thermocline depths during the boreal summer season, when monsoon winds blow from the southeast (Sprintall et al., 2009). Based on these modern observations, we may expect that some ITF modulation exists at orbital timescale, owing to the strong imprint of precession on long-term SE monsoon wind dynamics (Lückge et al., 2009; Mohtadi et al., 2011a). But such a link is not clearly seen in paleo-ITF records. Paleo-climatic reconstructions suggest, for instance, that the strength of SE monsoon winds was at a maximum during the early

Holocene (~10ka), when boreal summer insolation reached a peak (Mohtadi et al., 2011a). Assuming that the insolation-driven enhancement of SE monsoon winds is transferred to ITF, a higher flux would be expected during the early Holocene. However, data support the opposite scenario. They show a high east-west TWT gradient in the Timor Sea, which was interpreted as reflecting a weakened ITF thermocline transport (Holbourn et al., 2011). This observation either indicates (1) SE monsoon wind intensity and ITF transport are decoupled on orbital timescale, or (2) that TWT gradients reconstructed along the Indonesian Archipelago do not accurately grasp the full variability of the past ITF flux. Given the complexity of oceanic circulation and vertical mixing within the Indonesian Archipelago, our contention is that the lateral ITF signature on TWT gradient could have been disturbed by the superimposition of local changes in temperature related to the development of seasonal upwelling or downwelling cells forced by monsoon winds.

In the present paper, we propose to address past ITF variability through a different strategy. Instead of reconstructing paleo-ITF variability based on the evolution of TWT-gradient along the main path of the ITF, we propose to disentangle the respective influence of upwelling and ITF on the TWT record of a site located in the SE part of the Java upwelling (core MD98-2165, Fig. 1). Our strategy is based on the comparison of the TWT evolution at this site with the evolution of TWT reconstructed in the nearby core SO139-74KL, located south of Sumatra, further away from a main ITF exit, and strictly under the influence of the Java-Sumatra upwelling (Wang et al., 2018).

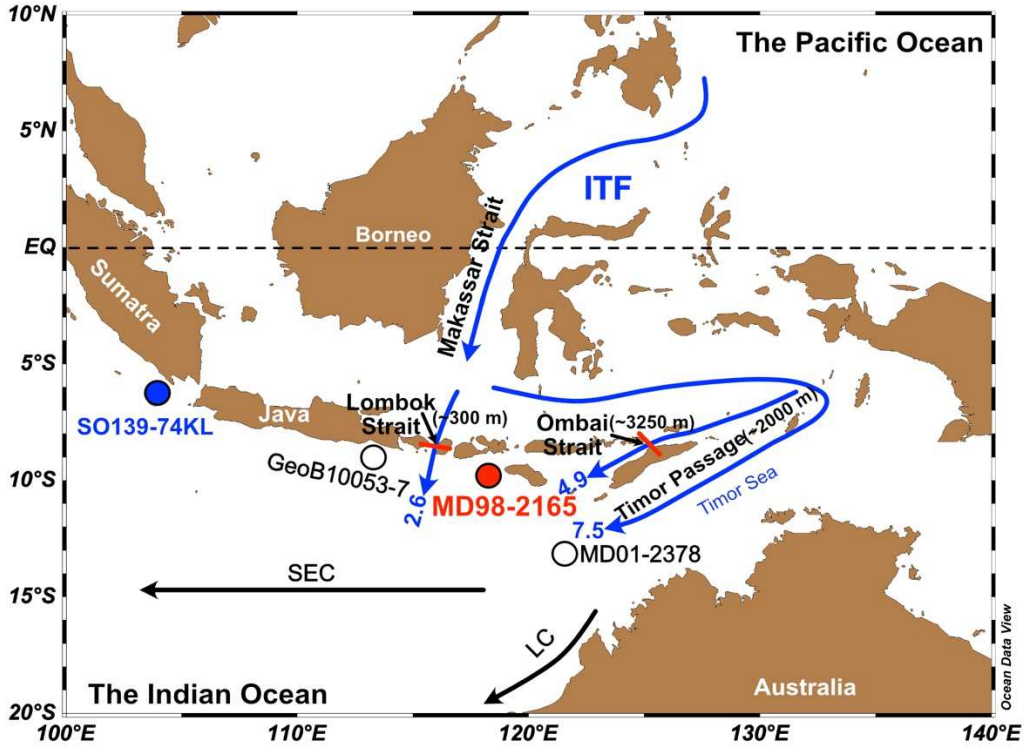

Fig. 1. Oceanic currents in the Indonesian Archipelago and Eastern Indian Ocean, and locations of sediment cores used in this paper: MD98-2165 (this study); SO139-74KL (Wang et al., 2018); MD01-2378 (Xu et al., 2008; Holbourn et al., 2011); and GeoB10053-7 (Mohtadi et al., 2011a). ITF = Indonesian Throughflow (blue line); LC = Leeuwin Current; SEC = South Equatorial Current. The three primary ITF exits — Lombok Strait, Ombai Strait and Timor Passage — are shown, with their sill depths (in brackets). The fluxes of ITF water being transported through each of these main exits is given in Sverdrup (1 Sv = 10^6 m^3 s^{-1}) on the map (blue numbers).

2. Modern oceanographic settings and past evolution of the Java upwelling

Core MD98-2165 is located to the southeast of Lombok strait and west of the Ombai Strait, two of the three main ITF exits in the eastern Indian Ocean (Fig. 1). The modern ITF transport is dominated by regional monsoon forcing, with maximum ITF flux occurring during the SE monsoon (boreal summer season) when the sea level is lowered by wind-driven, offshore Ekman transport along the south coast of Java (Sprintall et al., 2009) . In addition to enhancing the ITF, the Ekman transport also bring to the subsurface cold waters from deeper depths, resulting in an upwelling zone characterized by cold TWT along the south coast off Java and Sumatra during the boreal summer season (Fig. 2; Susanto et al., 2001).

As can be seen from Fig. 2, core MD98-2165 is located to the East of the Java upwelling. Core SO139-74KL, on the other hand, is located to the west of the Java upwelling. At site SO139-74KL, further away from the main ITF exits, TWT is mainly controlled by

upwelling dynamics (Kuswardani and Qiao, 2014; Wang et al., 2018). In contrast, at the site of MD98-2165, located in the ITF outflow region, TWT is under the combined effects of the Java upwelling dynamics and the ITF transport, with upwelling being the dominant forcing of seasonal TWT changes at both sites. The strong impact of the upwelling can be readily seen from the seasonal maps of TWT (Fig. 2a-b) and the strong co-variance between monthly-averaged TWT records from sites MD98-2165 and SO139-74KL (taking the period 1995 to 2015 and 100 m water depth as an example; Fig. 2c). At both sites, a characteristic low in TWT takes place during the SE monsoon season (boreal summer; Fig. 2c). This low is associated with the period of maximum upwelling intensity along Java and Sumatra. As can be seen in Fig. 2c, the difference in TWT between the two sites is relatively small during this upwelling season (less than 1 °C), and larger during the non-upwelling season (up to 2.5 °C). The in-phase covariance of TWT at both sites, chiefly resulting from the upwelling dynamics, can be readily seen also in the multi-annual TWT variability recorded over the same 20-year period (1995 to 2005, Fig. 2d). As is shown in Fig. 2d, amplitude of temperature changes at the site SO139-74KL is usually stronger than at the site MD98-2165, with higher temperatures at SO139-74KL than MD98-2165 during boreal winters (non-upwelling season) and colder temperatures during the boreal summers (active upwelling). The lower amplitude of TWT changes at the site MD98-2165 likely results from the moderating impact of the ITF advection, which tends to warm the thermocline waters during the upwelling season, but cool them slightly down during the non-upwelling season, because ITF thermocline waters have a lower temperature than their Indian Ocean counterparts (Gordon, 2005).

The underlying mechanisms that control the inter-annual ITF variability are still unclear. Recent studies concluded about the highly complex nature of that variability. It is thought to be associated with a combination of El-Niño Southern Oscillation (ENSO) and Indian Ocean Dipole forcing (Sprintall and Révelard, 2014). Today, the inter-annual evolution of TWT at MD98-2165 results from a combination of upwelling dynamics and ITF variability (temperature and/or flux), with the ITF impacts being relatively small compared to the upwelling influence. Previous studies have shown that strong changes in ITF occurred at millennial to multi-orbital timescales (Fan et al., 2018; Holbourn et al., 2011; Zuraida et al., 2009). Our main objective, in the present paper, is to study the long-term evolution TWT at the exit of the Indonesian Archipelago, at the site MD98-2165, and try to disentangle the potential effects of upwelling and ITF at orbital and glacial-interglacial timescales.

Sediment trap and core top studies indicate that the foraminiferal species *Pulleniatina obliquiloculata* lives in upper thermocline depth between 60 and 100 m in the Java-Sumatra upwelling region (Fig. 2e; Mohatdi et al., 2009; Mohtadi et al., 2011b). Owing to the higher flux of foraminifera during the upwelling season, shell geochemistry (e.g., $\delta^{18}O$ and Mg/Ca) of *P. obliquiloculata* tends to record the upper thermocline conditions of the upwelling season (July to October; Mohatdi et al., 2009; Mohtadi et al., 2011b). Based on *P. obliquiloculata* Mg/Ca-derived TWT, Wang et al. (2018) showed recently that paleo-TWT had always been chiefly controlled by upwelling variations on orbital timescale over the late Quaternary at the site SO139-74KL. In this study, we used the same approach (i.e., Mg/Ca ratio measured on the thermocline dwelling species *P. obliquiloculata*) to reconstruct past TWT variations at site MD98-2165.

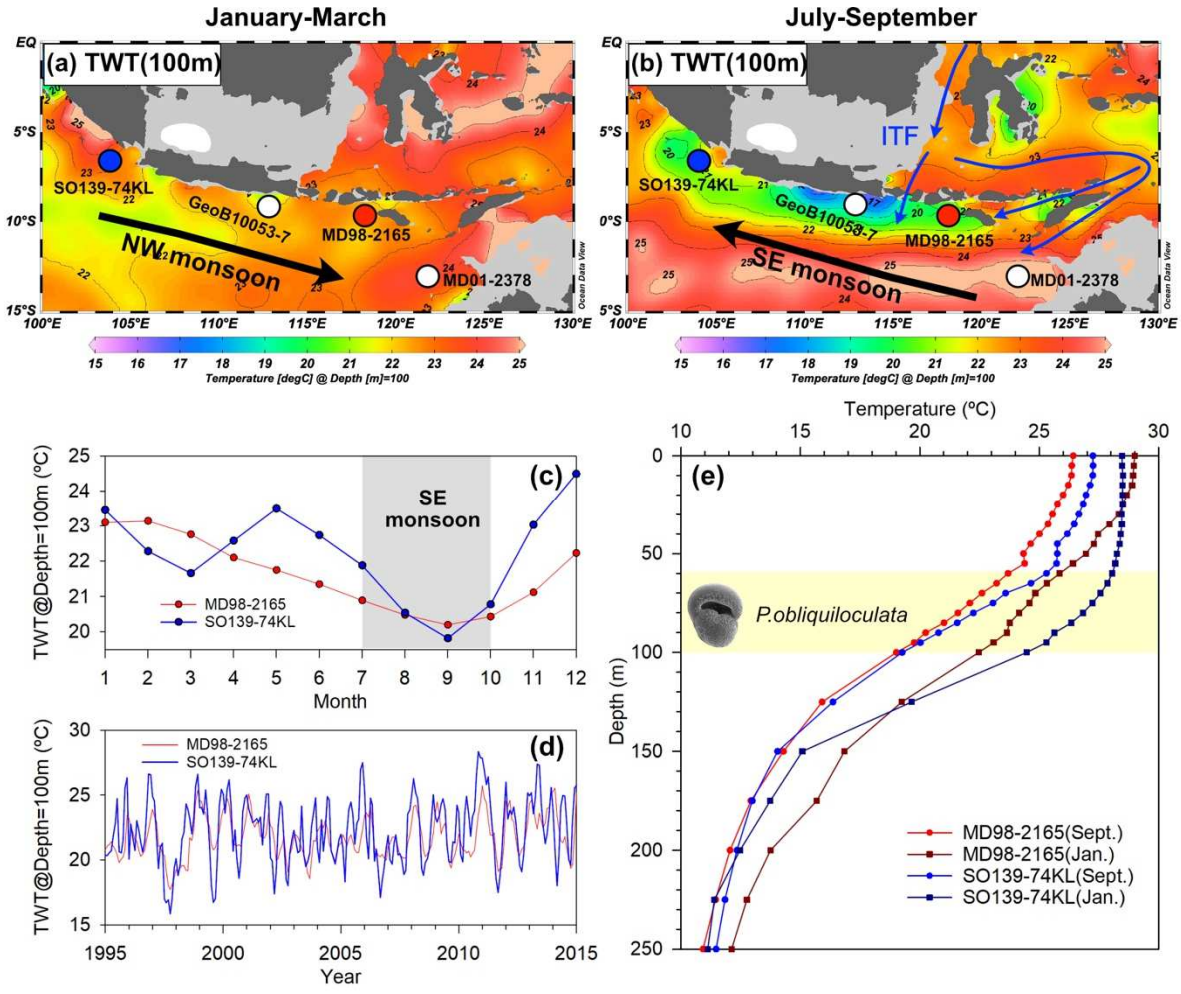

Fig. 2. Modern oceanographic settings in the studied area. (a) and (b) show the water temperature distribution at a depth of 100 m (maximum ITF transport depth, Sprintall et al., 2009) averaged over the January to March season ((a) NW monsoon season) and over the July to September season ((b) SE monsoon season). Datasets are from WOA13 (Locarnini et al., 2013). The locations of sediment core MD98-2165 (red dot), SO139-74KL (blue dot), MD01-2378 (white dot) and GeoB10053-7 (white dot) are also shown. Black arrows in (a) and (b) indicate the prevailing seasonal wind direction; blue arrow in (b) represents the ITF.

(c) Monthly evolution of TWT (100 m of water depth) averaged over the latest 20 years (1995-2015) available in Simple Ocean Data Assimilation (SODA) database (Carton and Giese, 2008) at sites MD98-2165 and SO139-74KL. The grey shaded area indicates the SE monsoon season. (d) Evolution of monthly thermocline water temperature (100 m of water depth) over the period 1995 to 2015 at sites MD98-2165 (red line) and SO139-74KL (blue line) from the same SODA database. (e) Depth profiles of temperature during different seasons at sites MD98-2165 and SO139-74KL. Horizontal yellow area indicates the habitat depth range of *P. obliquiloculata* in the Java-Sumatra upwelling region.

3. Material and methods

3.1 Sediment core MD98-2165 and age model

Sediment core MD98-2165 (9.65S, 118.34E) was retrieved at a water depth of 2100 m to the southeast of the Lombok Strait and southwest of the Ombai Strait (Fig. 1). The core was obtained during the Images IV cruise of the French R/V *Marion Dufresne*. It is 42.3 m long, the upper 34.5 m are studied in this paper . Previous analyses on this core include 20 accelerator mass spectrometry (AMS) ^{14}C dates at several depth intervals between 0 and 800 cm (Waelbroeck et al., 2006), and high-resolution oxygen isotope records from both planktonic (*Globigerinoides ruber*) and benthic (*Cibicides wuellerstorfi* and *Hoeglundina elegans*) foraminifera along the whole core (Levi, 2003; Levi et al., 2007; Waelbroeck et al., 2006). These data were used to construct the age model and oxygen isotope stratigraphy.

An initial age model had been constructed by using absolute radiocarbon ages and benthic $\delta^{18}O$ foraminiferal stratigraphy (Levi, 2003; Levi et al., 2007; Waelbroeck et al., 2006). In this initial age model, calendar ages were computed using MARINE98 calibration curve (Waelbroeck et al., 2006). Here, we updated the radiocarbon calendar ages by using the latest MARINE20 calibration curve (Heaton et al., 2020). We set the local marine reservoir age (ΔR) to -117 ± 70 years based on a modern measurement in the Java-Sumatra upwelling region (Southon et al., 2002). In between dated control-points, the conversion of depths to ^{14}C-derived calendar ages was made using the Bayesian statistical methodology of Bacon (Blaauw et al., 2011). For this upper core section (down to 774 cm), the absolute age uncertainties (2σ) are generally less than 0.5 ka.

For the lower part of the core (774 – 3889 cm) , we establish a new depth-age model by aligning the benthic $\delta^{18}O$ record of MD98-2165 to global benthic $\delta^{18}O$ stack. We used the LR04 stack (Lisiecki and Raymo, 2005) for the interval 270-150 ka, and the revised LS16 stack (Lisiecki and Stern, 2016) for the interval 150-0 ka. We used the HMM-Match MATLAB code (Lin et al., 2014) to automatically align benthic $\delta^{18}O$ record of MD98-2165 to the global benthic stack. This HMM-Match MATLAB code provides 95% confidence for

220 $\delta^{18}O$ alignment by using a hidden Markov model probabilistic algorithm (Lin et al., 2014). It
221 is worth to note that these age uncertainties only take into account alignment uncertainties
222 and not including the age uncertainties of $\delta^{18}O$ stacks used as targets. As can be seen in Fig.
223 3b, the alignment age uncertainties are generally lower than 2 ka in the interval of 300 – 60
224 ka due to the high similarity between our benthic $\delta^{18}O$ and the global stacks. However, in the
225 interval 60 – 25 ka the alignment age uncertainties increase dramatically and reach a
226 maximum of ~ 6 ka. This is mainly due to the target and the MD98-2165 $\delta^{18}O$ records
227 showing more differences, with many more details and variability in the benthic $\delta^{18}O$ record
228 of MD98-2165. Over this interval, MD98-2165 benthic $\delta^{18}O$ shows five peaks, whereas there
229 are only four in the global stack (Fig 3 a). The depth-age model for this interval was thus
230 simply obtained by assuming a constant sedimentation rate between 60 ka (1252 cm, the last
231 control-point for which there is no ambiguity in the correction with the $\delta^{18}O$ stack) and 25.3
232 ka (774 cm, the oldest ^{14}C date). This modification clearly increases the visual fit between
233 the benthic $\delta^{18}O$ of MD98-2165 and the global stack (Fig. 3 c).

234 Based on the depth-age model, the average sedimentation rate is ~ 13 cm/ka (Fig. 3 d).
235 From 300 to 20 ka — the interval over which the age model is mainly based on $\delta^{18}O$
236 alignment — the sedimentation remains relatively constant around 10 cm/ka. From 20 to
237 present, the estimated mean sedimentation rate increases dramatically from ~10 cm/ka to ~70
238 cm/ka. Part of that increase is likely associated with the elastic rebound of the coring cable
239 and the resulting over-sampling of upper sediments during the early phase of coring
240 (Szeremeta et al., 2004). Oversampling during giant coring was not properly corrected during
241 the early IMAGES cruises.

242 **Table 1.** AMS ^{14}C dates and corresponding calendar ages of core MD98-2165

Composite depth (cm)	^{14}C age ± 1σ (years BP)	Calendar age (years BP)	95% (2σ) confidence interval (years BP)
55	1150 ± 40	653	381 - 907
135	2210 ± 40	1772	1498 - 2084
213	3210 ± 40	3012	2744 - 3312
260	3910 ± 90	3851	3513 - 4228
320	4740 ± 110	4949	4548 - 5352
460	7500 ± 110	7941	7577 - 8388
560	10340 ± 120	11531	11050 - 12069
600	11430 ± 130	12880	12526 - 13245
620	12100 ± 130	13638	13289 - 14222
640	13040 ± 150	14856	14257 - 15395

656	13590 ± 140	15734	15296 - 16215
664	14050 ± 120	16251	15951 - 16565
674	14360 ± 140	16896	16490 - 17359
680	15080 ± 160	17352	17029 - 17698
690	15660 ± 130	18138	17765 - 18483
698	16030 ± 140	18761	18351 - 19259
740	19780 ± 170	22960	22264 - 23571
774	22330 ± 220	25272	23557 - 26053

243 ** ^{14}C dates were taken from Waelbroeck et al. (2006).*

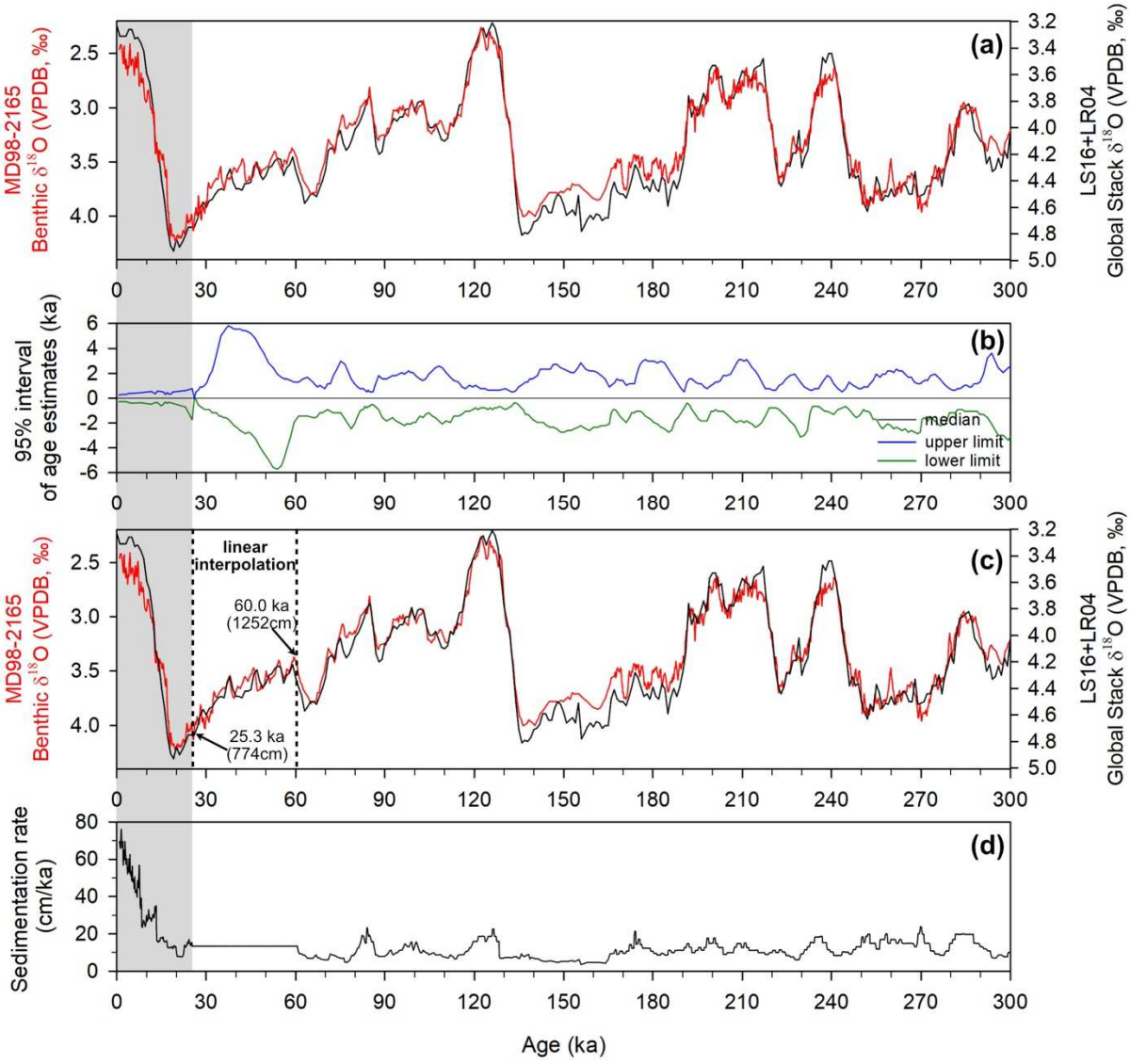

244

245 **Fig. 3.** Age model of MD98-2165. (a) Comparison between MD98-2165 benthic $\delta^{18}O$ and the
246 global stack. The chronology in the 0 – 25ka interval is based on radiocarbon ages (gray bar
247 interval), while in the 25 – 300 ka interval it is based on $\delta^{18}O$ alignment. (b) The 95%
248 confidence band around the median; calculated through a Bacon approach in the 0 – 25 ka
249 interval (gray bar interval); and estimated in the HMM-Match alignment over the 25 – 300 ka
250 interval. (c) Comparison between MD98-2165 benthic $\delta^{18}O$ and the global stacks. 0 – 25 ka

based on radiocarbon ages (gray bar interval); 25 – 60 ka based on linear interpolation between 25 ka (774 cm) and 60 ka (1252 cm); 60 – 300 ka based on $\delta^{18}O$ alignment. (d) Sedimentation rates. Gray bar indicate interval which age model is established by absolute radiocarbon ages.

3.2 Mg/Ca measurements

For measuring *P. obliquiloculata* Mg/Ca ratio, core MD98-2165 was sampled at 4-12 cm interval in the 110-3450 cm depth interval, corresponding to 1.5 – 270 ka. Samples were dried and weighted. Samples were then washed over a 63 µm sieve. Residuals were dried on a sheet of filter paper. About 30 tests of *P. obliquiloculata* were picked from the 250-355 µm size fraction. Foraminiferal tests were gently crushed between two glass plates under a binocular. Crushed tests were then transferred to acid-cleaned 500 µl centrifuge tubes for further cleaning. Samples were cleaned following the method described in (Barker et al., 2003). After cleaning, each sample was dissolved within 0.075M HNO_3 and then centrifuged for removing undissolved particulate impurities. The supernatant solution was transferred to a new acid-cleaned 500 µl centrifuge tube. Mg/Ca ratio were measured using an inductively coupled plasma mass spectrometry (ICP-MS, Analytik Jena PlasmaQuant MS Elite), and as well as for Al/Ca, Mn/Ca and Fe/Ca for examining the cleaning efficiency on clay contamination and post-depositional Mn-rich oxide coatings. Aliquots of samples were first analyzed for Ca concentrations and the remaining solutions were diluted to reach a Ca concentration around 100 ppm for all the samples in order to minimize possible matrix effects. For the calibration of Mg/Ca analyses, we used a series of six standard solutions with Ca concentration around 100 ppm and Mg/Ca ratios covering the range of values commonly observed in foraminiferal calcite: Standard 1 = 0.64 mmol/mol, Standard 2 = 1.66 mmol/mol, Standard 3 = 2.63 mmol/mol, Standard 4 = 3.69 mmol/mol, Standard 5 = 5.23 mmol/mol, Standard 6 = 7.72 mmol/mol. Standard 3 being used as our drift-correction solution was analyzed every 3 samples for monitoring the instrument variability and correcting samples after the analysis. The long-term reproducibility of Mg/Ca measurements obtained by replicating analyses Standard 4 solution is ±1.4% (1σ). This estimation is based on 144 analyses performed during 24 working sessions over a one-year period. No relationship was observed between Mg/Ca and Mn/Ca, Fe/Ca or Al/Ca variations. Thus, no Mg/Ca data was rejected from our dataset.

3.3 Conversion of Mg/Ca ratios to temperatures and consistency of datasets

Mg/Ca-based TWT were compared between different sediment cores in this study. As shown in Table 2, the Mg/Ca from the different studies were measured from slightly different

foraminifera shell sizes and by using different cleaning methods. Xu et al. (2010) demonstrated that for *P. obliquiloculata* species the specimens picked from the 250-315 µm and >315 µm size fractions do not exhibit significant Mg/Ca differences. However, the use of different cleaning methods for Mg/Ca analysis, specifically with or without a reductive step designed to remove oxide coating, leads to different Mg/Ca-based temperature estimates (Barker et al., 2003; Pang et al., 2020; Rosenthal et al., 2004). It has been shown that the reductive cleaning step can decrease the Mg/Ca ratios by a few percent compared to values obtained after a non-reductive cleaning.

We performed a detailed study of cleaning effects on Mg/Ca temperatures obtained on core MD98-2165 samples. Our results show that applying a reductive step decreases the Mg/Ca ratio of *P. obliquiloculata* by 4% compared to the non-reductive cleaning method (Pang et al., 2020). In order to minimize the cleaning method bias when comparing our Mg/Ca-TWT with those from other studies which used a reductive step in their cleaning strategy, the reductively cleaned Mg/Ca datasets (listed in Table 2) were corrected by +4%. Such cleaning-offset correction does not alter the relative temperature variations along each core.

The Mg/Ca ratio measured by this study and those from other studies (listed in Table 2) were converted to temperatures by using the same calibration equation developed by (Anand et al., 2003): $Mg/Ca = 0.328 \exp(0.09*T)$ for *P.obliquiloculata*. When using this calibration, the +4% correction for the reductively cleaned Mg/Ca datasets leads to a +0.45°C shift in temperature. The total uncertainty in Mg/Ca-TWT reconstruction for core MD98-2165 (this study) was estimated by propagating the uncertainties introduced by Mg/Ca measurements and Mg/Ca temperature calibration. This total uncertainty is on average about ±1°C (1σ) .

Table 2. Sediment cores used in this study.

Core ID	Lat./Long. (water depth)	Species (size)	Cleaning*	Reference
MD98-2165	9.65 S, 118.34 E (2100m)	*P. obliquiloculata* (250-350 µm)	NRC	This study
SO139-74KL	6.54 S, 103.83 E (1690m)	*P. obliquiloculata* (350-450 µm)	RC	Wang et al., 2018
MD01-2378	13.08 S, 121.79 E (1783m)	*P. obliquiloculata* (250-315 µm)	RC	Xu et al., 2008

**NRC :non-reductively cleaning method; RC : reductively cleaning method.*

4. Results

The *P. obliquiloculata* Mg/Ca and the estimated TWT from MD98-2165 are shown

versus age in Fig. 4. Mg/Ca ratio of *P.obliquiloculata* vary between 1.6 and 3.1 mmol/mol, corresponding to TWT ranging between 17.8 ± 0.9 and 25.1 ± 1.2 °C. The core top TWT (at ~1.5ka) is ~ 20.4 °C, which is identical, within the reconstructed TWT uncertainty, to modern mean temperature of ~ 20.6°C during the SE monsoon season at the water depth of 100 m. TWT variations show some similarities compared to the benthic $\delta^{18}O$ records at the glacial-interglacial timescale, such as a long-term cooling trend from MIS5e to MIS2 and rapid, high amplitude warmings during the benthic $\delta^{18}O$ terminations. The amplitude of glacial-interglacial TWT changes is ~3.3 ± 1.5 °C for Termination-III (T-III, transition MIS8/MIS7), 4.6±1.5 °C for T-II and 5±1.5 °C for T-I. Although they show some similarities at the glacial-interglacial timescale, TWT are not always warmer during interglacial than glacial periods. For example, during the Holocene, TWT decreases by up to 4°C towards present (from ~ 23.8°C at ~11 ka to ~19.8 °C at ~2.5 ka), which leads to the TWT in late MIS 1 being similar and even colder than some of the TWT reconstructed for glacial periods. This pattern is also observed in MIS 7 and MIS 5. These results suggest that TWT changes at site MD98-2165 do not strictly follow the global climate variations embedded in the $\delta^{18}O$ record, but contain a strong regional/local imprint.

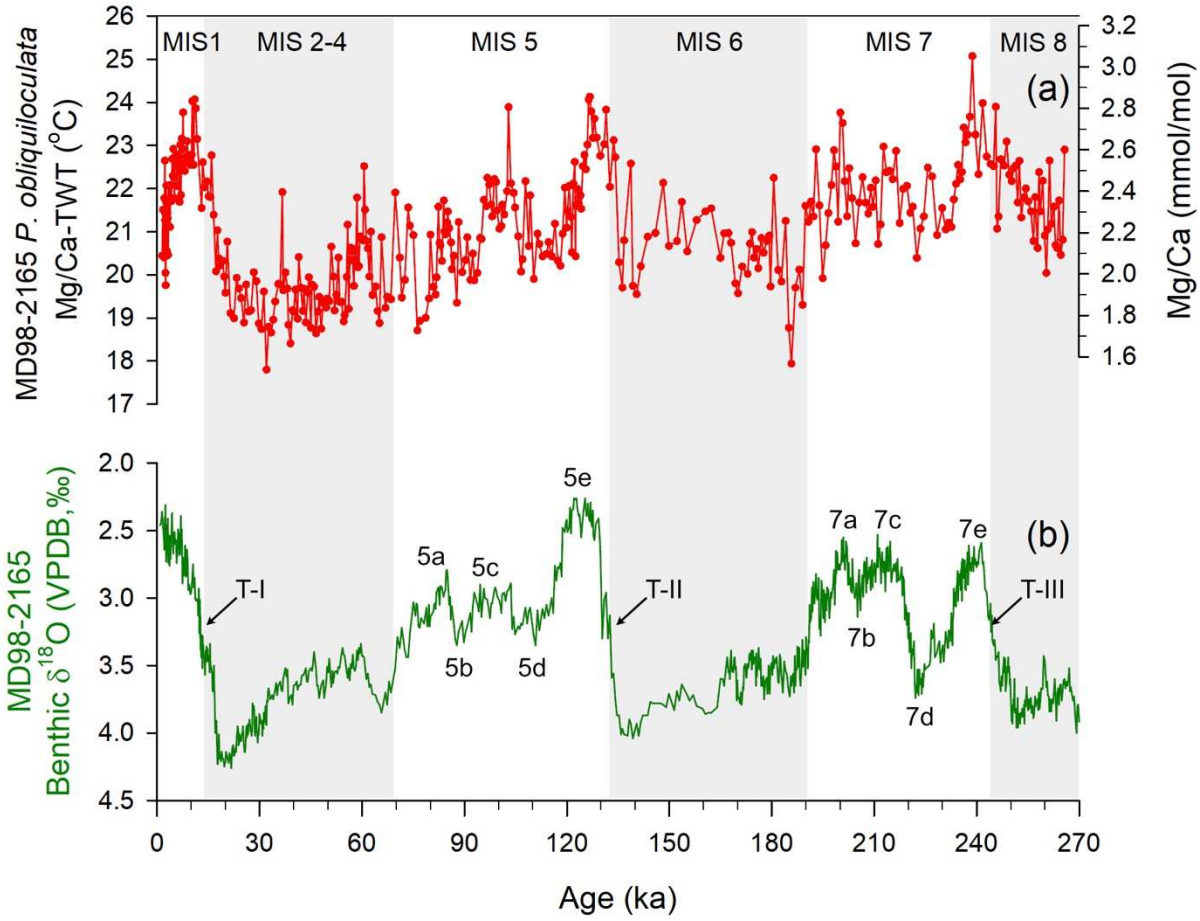

Fig. 4. Paleoclimate records of core MD98-2165. (a) *P. obliquiloculata* Mg/Ca-derived TWT. (b) Benthic $\delta^{18}O$ record of MD98-2165 as a stratigraphic reference (Levi, 2003; Waelbroeck et al., 2006). MIS stands for Marine Isotope Stage. Sub-stages of MIS5 (5a-5e) and MIS7 (7a-7e) are also marked. T-I, T-II and T-III mark the glacial terminations.

5. Discussion

5.1 Disentangling the impacts of vertical mixing (upwelling) and lateral advection (ITF) on the TWT of site MD98-2165, South of Lombok

As aforementioned, the site of core MD98-2165 is under the influence of two of the three main ITF exits in the Indian Ocean. Seasonal TWT variations at this site are linked to the dynamics of the wind-driven Java upwelling (Fig. 2; Susanto et al., 2001), with the ITF likely acting as a moderator, smoothing out the amplitude of TWT changes compared to TWT changes at the site of core SO139-74KL, within the core of Java-Sumatra upwelling. The ITF probably also explains part of the interannual TWT variability at site of MD98-2165, in particular through the combined influence of ENSO and IOD changes (Sprintall and Révelard, 2014; Susanto et al., 2001).

Marine sediment records have shown that, on the long, millennial to orbital timescales, the SE monsoon winds have always been a permanent feature of atmospheric circulation in this region (Lückge et al., 2009; Mohtadi et al., 2011a; Steinke et al., 2014). Furthermore, the detailed study of core SO139-74KL concluded that TWT changes at this site have been always controlled by the upwelling dynamics under the influence of SE monsoon wind intensity (Wang et al., 2018). These observations suggest that seasonal variability at the site of our core MD98-2165 has most likely been always under the influence of the upwelling dynamics. And the long-term variability at the site of MD98-2165 should show a combination of upwelling and ITF impacts.

In order to disentangle upwelling and ITF components, we compare in Fig. 5 the last 25 ka evolution of TWT at our site with that of TWT from core SO139-74KL located in the west of Java upwelling and away from the ITF outflow region (Wang et al., 2018) and from core MD01-2378 located in the center of the Timor Sea main exit, away from the upwelling system (Holbourn et al., 2011; Xu et al., 2008). These two sites represent end-members for TWT variability near our site: with and without the influence of the upwelling system. Concentrating on the last 25 ka makes it possible (i) to achieve a comparison over an interval with robust ^{14}C-based age models, and (ii) to focus on a key time period spanning from the last glacial maximum to the later Holocene, and characterized by a peak in boreal summer insolation at ~10 ka. In Fig. 5 we also display a proxy of upwelling intensity (% *Globigerina bulloides*), obtained from core GeoB10053-7, located in the heart of the Java upwelling (Fig 1 and 2; Mohtadi et al., 2011a).

As shown in Fig. 5, from 25 to about 16 ka, TWT of MD98-2165 were similar to TWT of SO139-74KL, but colder than TWT from MD01-2378, located outside the upwelling zone. This indicates that the upwelling dominated the TWT of MD98-2165 while the ITF exerted only a weak influence. This observation is in rather good agreement with the study of Fan et al. (2018), which suggested a weakened ITF during 27- 24.2 and 19-13.4 ka. By contrast, from ~16 to 4 ka, the TWT of MD98-2165 were much warmer than TWT of SO139-74KL and comparable to TWT of MD01-2378. Over this period, higher percentages of *G. bulloides* in core GeoB10053-7 indicate that the upwelling along Java was much stronger than today, suggesting enhanced local SE monsoon winds (Mohtadi et al., 2011a). This stronger SE monsoon wind signal is clearly imprinted in the TWT record of core SO139-74KL through the responsible change of upwelling intensity at this site to the SE winds, which shows its minimal values during the early Holocene, coeval with the peak

in *%G. bulloides* (Fig. 5). However, our data indicate that in this context of enhanced SE monsoon winds, the TWT record at site MD98-2165 varied opposite to that of SO139-74KL, showing maximum temperature values at ~10ka, about ~ 6°C higher than the TWT at site SO139-74KL, and close to MD01-2378 values. This suggests that, contrary to what we observe at site SO139-74KL, enhanced wind-driven Ekman offshore transport did not result in decreased TWT at site MD98-2165. This indicates that TWT during the early Holocene was dominated by an enhanced, lateral ITF transport of warm water rather than by the upwelling of cold water. The TWT of MD98-2165 during the early Holocene was nearly 4°C higher than during the glacial time (taken at ~ 20 ka for reference) and the later Holocene (at ~1.5ka). From 4 ka towards the present, TWT from core MD98-2165 tend to become progressively similar to those from the upwelling site SO139-74KL, varying along with the boreal summer insolation. This implies that the influence of ITF at the site of core MD98-2165 gradually weakened towards the present.

Our observations suggest that, during the early Holocene peak in boreal summer insolation, when SE monsoon winds and upwelling intensified, the ITF thermocline water was warmer and its flux was stronger. The increase of ITF thermocline water temperature can be readily deduced from the co-evolution of TWT at the site of MD01-2378 and MD98-2165, which show positive correlation with boreal summer insolation. This temperature evolution likely results from the fact that ITF waters chiefly originate from the North Pacific Ocean where temperatures are controlled by boreal summer insolation (Bolliet et al., 2011; Dang et al., 2012). The stronger ITF flux during the early Holocene is suggested by the evolution of MD98-2165 temperatures, which increased while the upwelling intensity increased, clearly indicating that ITF became dominant, overwhelming the influence of the upwelling and driving thermocline temperatures from MD98-2165 closer to those from the Timor Sea site MD01-2378.

As aforementioned, modern observations tie the dynamics of the Java-Sumatra upwelling and seasonal ITF changes to summer insolation forcing, through the SE wind dynamics. Our observations suggest that such a control is also acting at orbital timescales, with changes in summer boreal insolation not only driving the upwelling dynamics (Wang et al., 2018), but also strongly modifying the thermocline ITF temperature and flux. Interestingly, at this orbital timescale, the ITF signal becomes dominant over the upwelling activity in controlling TWT of MD98-2165, whereas modern data indicate that, at seasonal timescale, the TWT variability is clearly dominated by upwelling variability (Fig. 2).

In Fig. 5c, we managed to synthetize the above observations by computing a record that takes into account the relative TWT changes at our three reference sites. The proxy, named %TimorTh (Timor Thermocline %), is designed to quantitatively address the degree of similarity between TWT at MD98-2165 with respect to (i) the upwelling site SO139-74KL and (ii) the non-upwelling site MD01-2378. After the three records were interpolated to the same constant time interval (1 ka), we computed at each age increment the TWT difference between SO139-74KL and MD98-2165 ($TWT_{MD98-2165} - TWT_{SO139-74KL}$), and normalized them with respect to the TWT difference between the Timor sea TWT (ITF end member) and the SO139-74KL TWT (upwelling reference; $TWT_{MD01-2378}$-$TWT_{SO139-74KL}$). The ratio is expressed as a percentage:

$$\%TimorTh_{MD98-2165} = (TWT_{MD98-2165} - TWT_{SO139-74KL}) / (TWT_{MD01-2378} - TWT_{SO139-74KL}) * 100.$$

When %TimorTh is close to 1 (i.e. TWT at our site is similar to that of MD01-2378), the influence of ITF is maximal, whereas when it is close to 0 (i.e. TWT at our site is similar to that of SO139-74KL), it is the upwelling that chiefly controls the thermocline temperature in the vicinity of Site MD98-2165. Age models for all the three TWT records over the last 25 ka are based on ^{14}C dates, the age model uncertainties (2σ) are less than 0.5 ka for each core (MD98-2165: Table 1 and Fig. 3; SO139-74KL: Lückge et al., 2009; MD01-2378: Xu et al., 2008). As we aim at using mainly the %TimorTh proxy to show the dynamic influence of ITF and upwelling at site MD98-2165 at orbital timescales, the relatively small age model uncertainties are not able to affect our conclusions.

As can be seen in Fig. 5c, the %TimorTh proxy clearly shows the orbital-driven signal embedded in the ITF variability. However, the proxy also emphasizes somehow a step-like evolution since the Last Glacial Maximum, with a rapid evolution from 23 to 16 ka followed by a more progressive change, almost a plateau, in the early Holocene (Fig. 5c). This plateau exists because TWT at site MD98-2165 and MD01-2378 become nearly similar in the interval younger than 16 ka. But, as can be readily seen from the Fig. 5b, the two temperature records continue to evolve, the temperature increasing at both sites to reach their maximum value at ~ 10 ka. Thus, the near plateau we observe in the %TimorTh profile above ~ 16 ka represents a "saturation" of the proxy. When the ITF flux increases, bringing the TWT of site MD98-2165 closer to those at site of MD01-2378, there exists a threshold above which any further increase in the ITF flux remains unseen because TWT at both sites are already similar. In the introduction of this paper, we suggested the existence of such a sensitivity problem for proxies based on the TWT difference between two sites located along

444 the main ITF path. This type of limitation is what we clearly observe, here, in the %TimorTh
445 proxy during termination I and the early Holocene.

446 The fact that TWT changes at orbital-scale are clearly different and somewhat anti-
447 correlated at site MD98-2165 and at site SO139-74KL, suggests an alternative way of
448 expressing the relative contribution of ITF: by considering simply the TWT gradient between
449 the two sites ($\Delta TWT = TWT_{MD98\text{-}2165} - TWT_{SO139\text{-}74KL}$). As can be seen (Fig. 5c) both
450 approaches clearly emphasize the orbital-related imprint in the ITF variability. However, the
451 approach based on the simple difference in TWT (ΔTWT) results in a smoother and more
452 gradual evolution over the studied 25-0 ka interval and does respect the full evolution of
453 TWT profiles, which peak at about ~ 10 ka. A higher-resolution study devoted to the 25-0 ka
454 interval will be necessary to dig further into similarities/differences between the two
455 approaches and resolve the sub-orbital variability. In the present paper, we focus only on the
456 long-term ITF dynamics by using the relative evolution of TWT at sites of MD98-2165 and
457 SO139-74KL. Although potential drawbacks may exist in the ΔTWT approach, the rather
458 good coherence between the ΔTWT and %TimorTh profiles suggest that the main source of
459 variability is indeed associated with ITF changes. Another additional advantage of the ΔTWT
460 approach is that by dealing only with two cores one also reduces the age-model uncertainties.

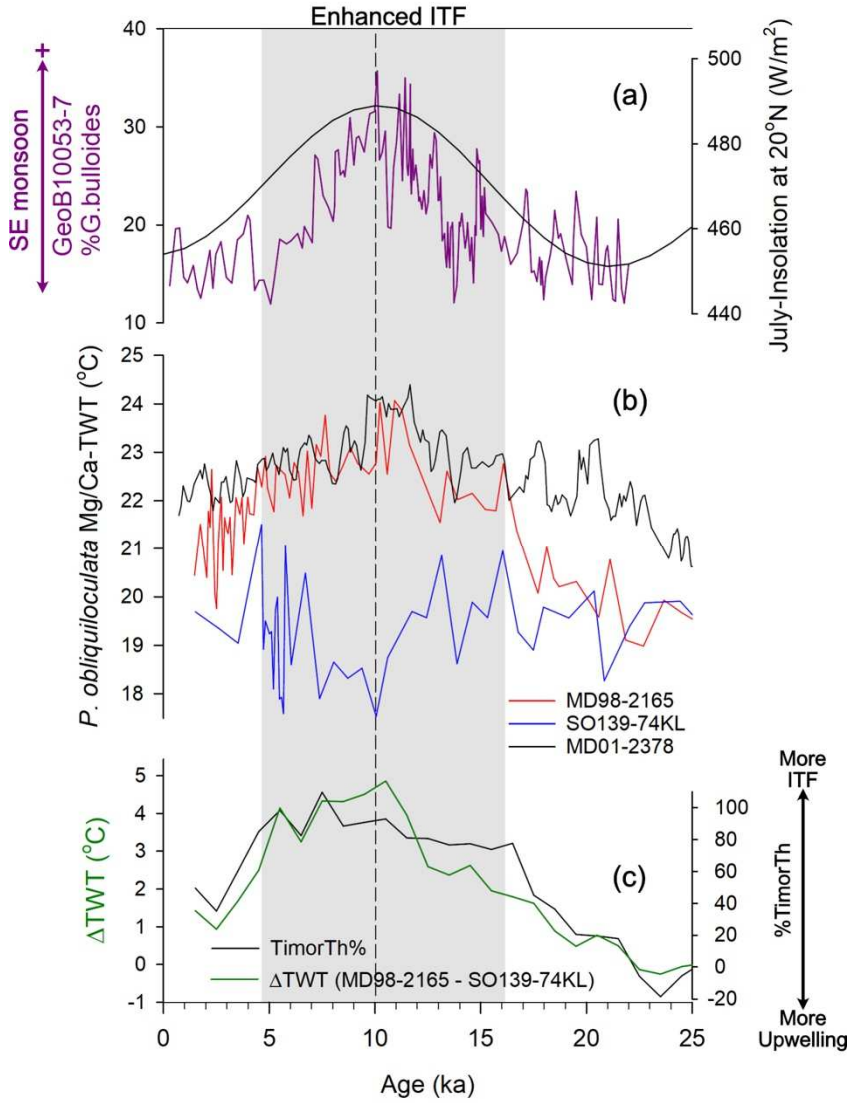

Fig. 5. Evolution of paleoceanographic records over the past 25ka. (a) Relative contribution (%) of *G. bulloides* in the foraminiferal assemblages of core GeoB10053-7 (dark purple line), a proxy of upwelling activity (large % of *G.bulloides* correspond to enhanced SE monsoon, and vice versa (Mohtadi et al., 2011a); And July insolation (black curve) at 20 ºN (Laskar et al., 2004). (b) *P. obliquiloculata*-derived TWT of MD98-2165 (red line, this study), SO139-74KL (blue line, Wang et al., 2018) and MD01-2378 (black line, Xu et al., 2008). (c) Estimation of relative contribution of ITF and upwelling on TWT at site MD98-2165 (%TWT, black curve; sea text for details), and difference between TWT at sites MD98-2165 and SO139-74KL (ΔTWT, dark green curve; see text for details).

5.2 Evolution of the ITF relative strength in response to precession-paced insolation forcing and sea level changes during the last 270 ka

As was already seen above for the 25-0 ka interval, the TWT record of MD98-2165 shows remarkable differences compared to the TWT record from core SO139-74KL (Fig. 6a). During MIS 7, MIS 5 and MIS1, TWT at site of core MD98-2165 were generally higher than at the site of core SO139-74KL. By contrast, the difference in TWT between these two core

sites were relatively small during MIS 6 and MIS 2-4 and, to a lesser degree, during MIS 8. Inside these glacial and interglacial intervals, the difference in TWT between the two sites also varies and suggests a strong orbital component.

We constructed a ΔTWT record over the full 270 ka interval. The TWT record from MD98-2165 has an average resolution of ~0.6 ka and cover the time period between ~ 1.5 and ~ 266 ka, whereas the TWT record from SO139-74KL has an average resolution of ~1.1 ka and cover the time period between ~ 1.5 ka and ~ 290 ka (Wang et al., 2018). After applying a three-point moving average, we interpolated linearly the TWT records of both cores to a constant 1.5 ka step from 1.5 ka to 265.5 ka. In order to estimate the impact of potential age model bias on the reconstructed ΔTWT profile during the periods without AMS ^{14}C dates, we used, both, the published age model for core SO139-74KL (Lückge et al., 2009), and a revised age model developed in this study by tuning the planktonic $\delta^{18}O$ record from SO139-74KL to the planktonic $\delta^{18}O$ record from core MD98-2165 (both obtained from *G. ruber*). The resulting ΔTWT records are shown in Fig. 6b. As can be readily seen, the two alternate age models only result in small differences between the ΔTWT profiles and, therefore, the same conclusions would be reached using either record as long as major changes in the ΔTWT evolution are concerned. In the rest of the manuscript, we used the ΔTWT record obtained with the revised age model of SO139-74KL.

In the top Holocene (i.e. 1.5 ka), the difference in TWT between the two sites is ~ 1°C. In order to facilitate the comparison with the upper Holocene situation, a reference line has been drawn at 1°C all along the ΔTWT profiles in Fig. 6b. As can be readily seen, the ΔTWT during cold stages MIS 6 and MIS 2-4 were generally lower than this upper Holocene ~ 1°C reference value, whereas ΔTWT during the warmer stages MIS 7, MIS 5 and the Holocene were higher, ΔTWT reaching up to ~ 6°C. The MIS 8 is a peculiar cold stage characterized by a relatively strong ΔTWT, greater than 1°C. The MIS 7d and MIS 5b sub-stages show low ΔTWT, very close to or even smaller than 1°C (Fig. 6b). Moreover, the ΔTWT record shows clearly cyclic variations inside glacial and especially interglacial stages. For example, large ΔTWT peak values repeatedly occur in warm substages of MIS 7 (a, c and e), MIS 5 (a, c and e) and as well as in the early Holocene (~10 ka). As already mentioned for the 25-0 ka interval, the decoupled and somewhat anti-phased TWT variability between MD98-2165 and SO139-74KL on orbital and glacial-interglacial timescales contrasts with the strong seasonal co-variance of TWT at the two sites, which is observed today (Figure 2). Based on the detailed observations made in the 25-0 ka interval, we conclude that ITF intensity was likely

stronger than for the upper Holocene during warm stages and sub-stages, and weaker during colder stages and sub-stages. This is in line with major conclusions reached by Holbourn et al. (2011) for ITF variability in MIS 5 and the MIS 4-2. Interestingly, our data suggest that the ITF intensity was apparently stronger during MIS 8 than for the late Holocene, whereas ITF intensity may have been similar to the late Holocene during MIS 7d and MIS 5b

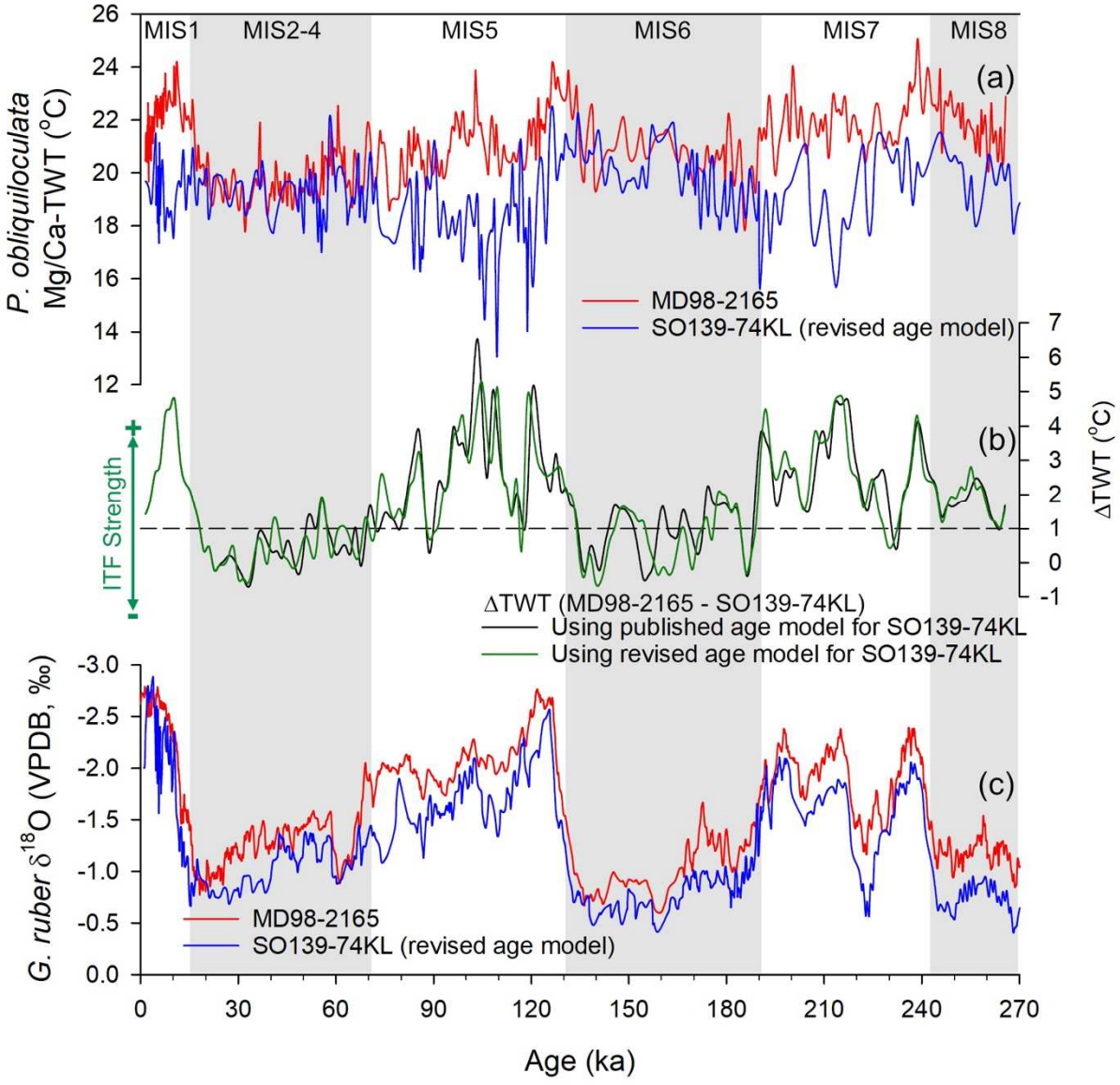

Fig. 6. Comparison of *P. obliquiloculata* Mg/Ca-derived TWT between core MD98-2165 and SO139-74KL. (a)TWT of MD98-2165 (red line, this study), TWT of SO139-74KL (blue line, Wang et al., 2018, on revised age model, see the text). (b) ΔTWT = TWT(MD98-2165)-TWT(SO139-74KL); ΔTWT in dark green line is calculated by using our revised age model for core SO139-74KL (see text for detail), ΔTWT in black line is calculated by using published age model for core SO139-74KL (Lückge et al., 2009); black dashed line is 1°C of ΔTWT served as a reference. (c) *G. ruber* $\delta^{18}O$ (after 3-point moving average) of MD98-2165 (red line, Levi, 2003) and SO139-74KL (blue line, Wang et al., 2018, on revised age

524 model).

525 We conducted spectral analyses in order to extract the quasi-cyclic variability
526 observed in the TWT records from core MD98-2165 and SO139-74KL and in the ΔTWT
527 profile. Spectral analysis reveals the presence of all the main orbital-like components (namely
528 eccentricity, obliquity and precession) above the theoretical red noise spectrum (Fig. 7a-b). It
529 suggests the strong role of the ~100 ka cycle, clearly above the 90% confidence level. This
530 long-term contributor has a period of ~ 135 ka in core MD98-2165 and ~ 100 ka in SO139-
531 74KL. The incoherency in the periodicity likely results from the relatively short length of the
532 records. With only ~ 270 ka, the core MD98-2165 record covers just two such ~ 135 ka
533 cycles, clearly suggesting a potential bias in the spectral analysis results. Although slightly
534 longer, the 290 ka-long TWT record of core SO139-74KL, does not provide either a good set
535 of data for deciphering the potential "eccentricity" component. Actually, a more thorough
536 examination of this ~ 100 ka cycle through band-pass filtering reveals that, in core SO139-
537 74KL, it is strongly associated to the almost linear trend in TWT seen between 170 and 70 ka.
538 Thus, it does not correspond to the usual glacial-interglacial ~ 100 ka oscillation, which is
539 seen for instance in planktonic foraminiferal $\delta^{18}O$ record (Fig. 6).

540 Interestingly, the obliquity component (~ 40 ka) is seen in the TWT record from core
541 MD98-2165 where it is even stronger than the 23-ka component (Fig. 7a), and it corresponds
542 only to a small ~ 36 ka peak in the TWT record from SO139-74KL, just above the red noise
543 spectrum level (Fig. 7b). The 23 ka cycle associated to precession is clearly seen in both
544 records, although it is below the 90% confidence level. The power spectrum of ΔTWT
545 reveals clearly 100-ka and 23-ka components (Fig. 7c), with the 23-ka component being
546 clearly enhanced in the ΔTWT. The fact that no obliquity component is seen in the ΔTWT
547 profile indicates that this signal is co-variant to a large extent in both TWT records and
548 cancels out when subtracting one TWT record from another.

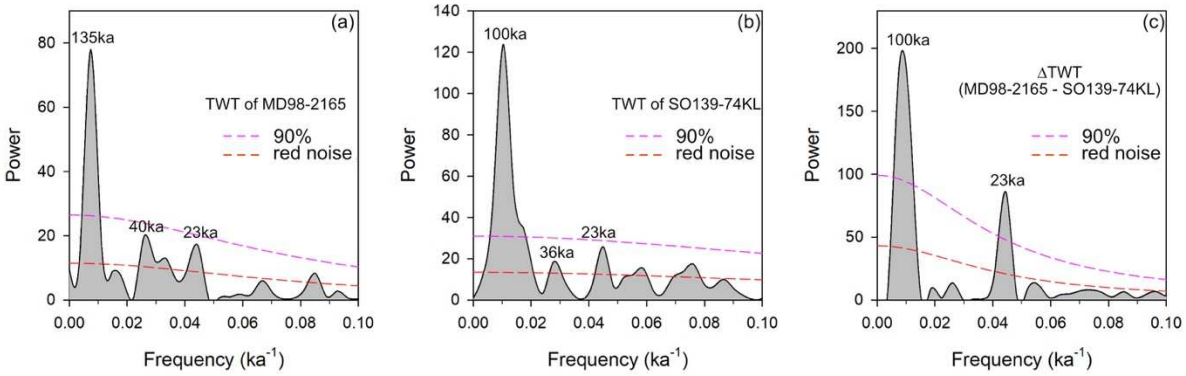

Fig. 7. Spectral analysis of TWT records from core MD98-2165 (a), SO139-74KL (b), and ΔTWT (c). Spectral analysis is conducted by using the REDFIT module from Past3 software (Hammer et al., 2001). The settings for the analysis are: Window = Welch, Oversample = 1 and Segments = 1; the red and pink dashed line indicate red-noise and 90% false-alarm level, respectively.

As expected, the 23-ka component from ΔTWT shows a strong resemblance with the precession signal (Fig. 8a). The enhanced precession-like component in ΔTWT compared to the two initial TWT records comes from the nearly anti-phased evolution of TWT at the 23-ka precession scale in core MD98-2165 and SO139-74KL (Fig. 8b), with increasing (decreasing) boreal summer insolation inducing decreased (increased) TWT at the site of SO139-74KL and increased (decreased) TWT at the site of MD98-2165. This result is in agreement with previous observations made over the last 25 ka interval (see above), which showed that when SE monsoon winds increased with increasing boreal summer insolation, they brought more cold water into the thermocline at site SO139-74KL by boosting the upwelling, but resulted in more warm water being carried at site MD98-2165 through enhanced ITF (and vice-versa). The persistent correlation between the ΔTWT with the boreal summer insolation over the last 270 ka (Fig. 9a) clearly indicates that the same mechanisms that we described over the last 25ka interval acted over the last 270 ka, resulting in the strong 23-ka precession component. It is our contention, therefore, that changes of ITF intensity flux and temperatures have been strongly influenced by precession-paced low-latitude insolation changes over the last 270 ka.

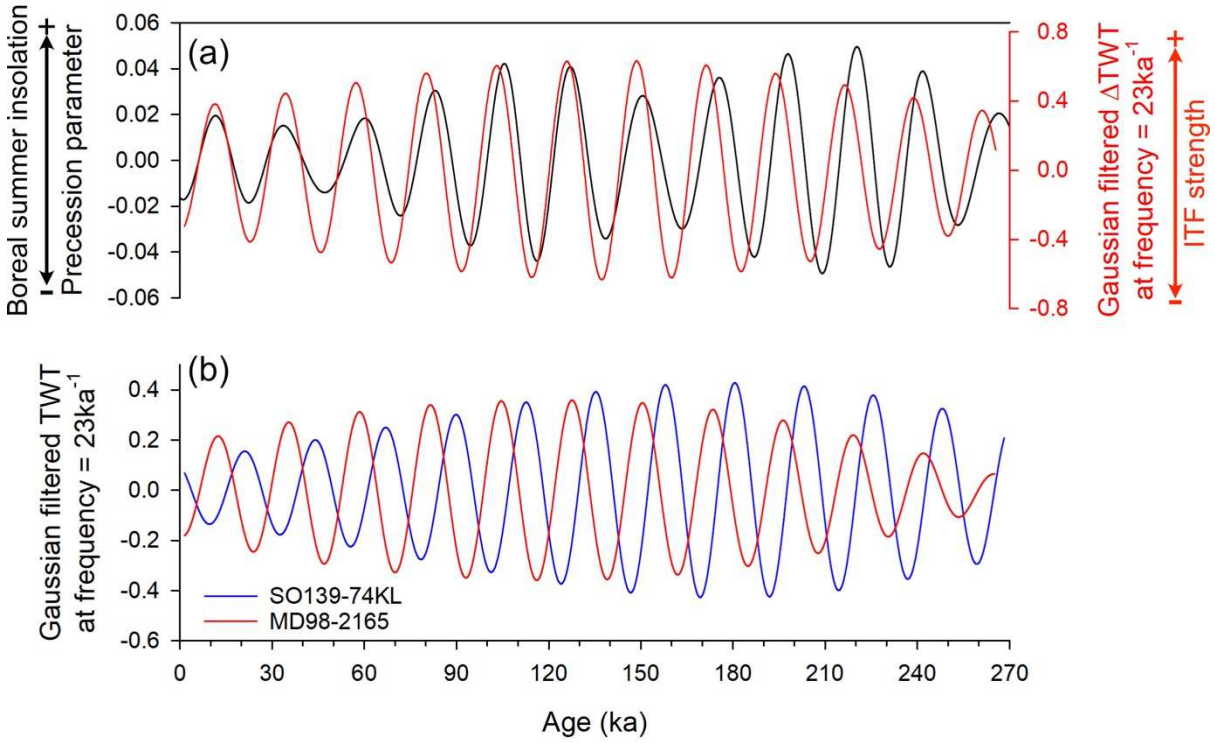

Fig. 8. Comparison of filtered proxy records with the precession parameter. (a) Comparison of precession parameter (black line) with the gaussian filtered ΔTWT at frequency = 23 ka^{-1} (red line). (b) Comparison of gaussian filtered TWT at frequency = 23 ka^{-1} between MD98-2165 (red line) and SO139-74KL (blue line). Gaussian filtering is conducted by using the software AnalySeries2.0 (Paillard et al., 1996), the filtering frequency center at 0.044 ± 0.003 ka^{-1} for all the TWT and ΔTWT records.

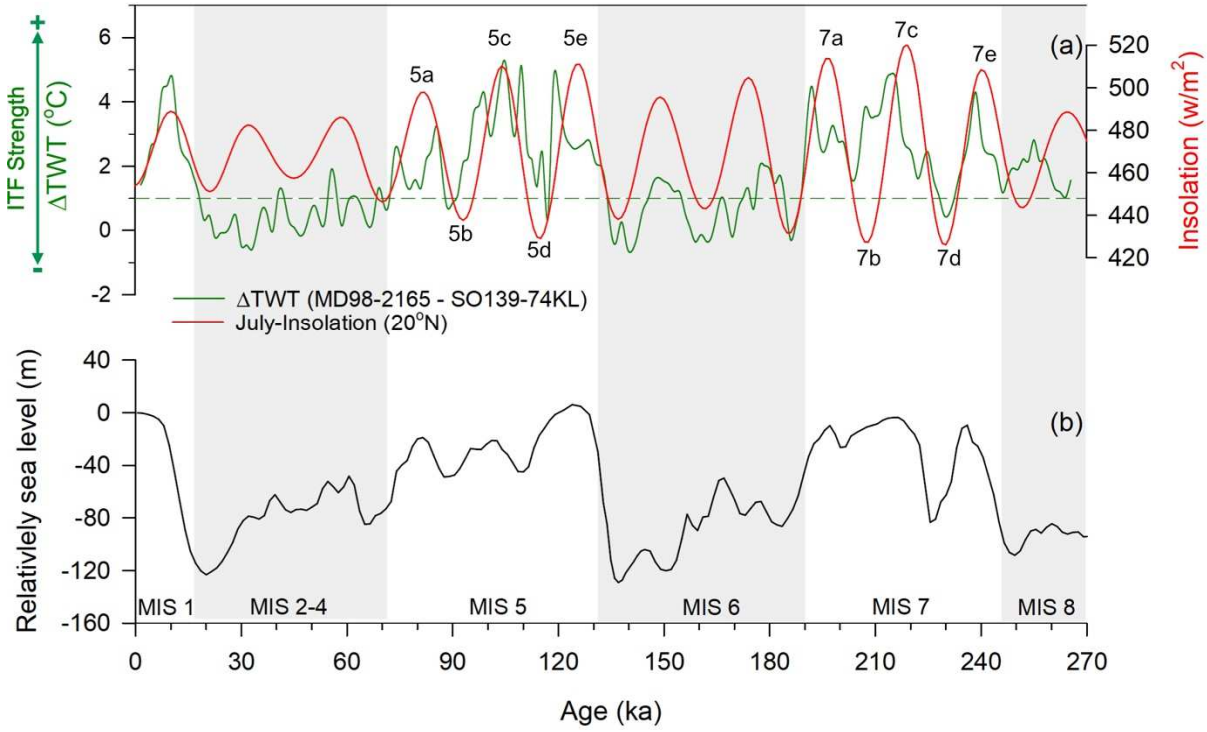

Fig. 9. Comparison of ΔTWT with boreal summer insolation and relative evolution of sea level. (a) The dark green curve is ΔTWT = TWT (MD98-2165) – TWT (SO139-74KL); the red curve is July insolation at 20°N (Laskar et al., 2004); substages of MIS 5 (5a to 5e) and MIS 7 (7a to 7c) are also marked. (b) reconstructed evolution of sea level changes (Waelbroeck et al., 2002).

The glacial-interglacial variability in ΔTWT can be seen through two different effects: (i) the average values are lower in MIS 6 and MIS 4-2, and (ii) the amplitude of ΔTWT variations are also reduced during these cold stages (Fig. 9a). This suggests that ITF was weakened and with a lower range of variability during glacial periods. As the Indonesian Archipelago is an area characterized by numerous islands and shallow sills, this glacial-interglacial variability of ITF may be associated to some extent with glacio-eustatic sea level variations. The lowered sea level, by exposing shallow shelves in the Indonesian archipelago, could have modified the land-sea thermal gradient and regional albedo, thus potentially influencing the ITF by modulating the SE monsoon strength in addition to orbital forcing (DiNezio et al., 2018). However, such scenario is undermined by the fact that no ~ 100-ka, glacial-interglacial component was found in the paleo-records of SE monsoon winds (Lückge et al., 2009; Wang et al., 2018). As an alternate hypothesis, the up to 120 m of sea level drop during glacial stages may have had an impact on the ITF flux by shallowing the ITF pathways especially at the Lombok Strait where the sill is only ~ 300 m depth at present (Fig.

598 1). It is likely that shallowed pathways reduced the thermocline ITF flux, and reduced both
599 the influence and variability of ITF on the TWT of site MD98-2165. However, this scenario
600 fails to explain the peculiar case of MIS 8, which despite being a glacial stage shows a
601 stronger ΔTWT (and thus, presumably, a stronger ITF flux) than during the late Holocene.

602 As none of these two scenarios can convincingly explain the general decrease of ITF
603 strength during glacial periods, another possibility would be that glacial-interglacial changes
604 of ITF are not controlled through regional sea-level effects but result from changes in the
605 thermohaline circulation and the global dynamics affecting the strength of surface and sub-
606 surface return branches of the Great Conveyor Belt. ITF eventually exits the Indian Ocean to
607 the Atlantic Ocean around the southern tip of Africa through the Agulhas leakage. The ITF
608 and the Agulhas leakage are thus the beginning and ending parts of the upper branch of the
609 Great Conveyor Belt in the Indian Ocean, respectively. Studies show that the Agulhas
610 leakage was largely reduced during glacial intervals, due to the northward migration of the
611 Southern Ocean subtropical front (Beal et al., 2011; Peeters et al., 2004). The reduction of
612 both the thermocline ITF and the Agulhas leakage during glacial periods, may indicate that
613 both mechanisms are simply the expression of a general weakening of the Great Conveyor
614 Belt return branch. However, whether there is indeed a causal relationship changes in the ITF
615 and Agulhas leakage is out of the scope of this study. Further studies are needed to confirm
616 the ITF variability at this glacial-interglacial timescale and explore the potential implications
617 and mechanisms.

618 ## 6. Conclusions

619 In this study, we presented a 270-ka long *P. obliquiloculata* Mg/Ca-derived TWT
620 record from core MD98-2165, located in the east of Java-Sumatra upwelling zone and in the
621 main ITF outflow region. Over the last 25 ka, we showed that the TWT record of MD98-
622 2165 oscillates between the pure, upwelling-driven TWT values from core SO139-74KL,
623 located in the west of Java-Sumatra upwelling, and a TWT record from the Timor Sea
624 (MD01-2378), away from the upwelling influence. The TWT gradient (ΔTWT) between the
625 upwelling site and our site can be used to decipher the relative strength of ITF through time.
626 The 270 ka-long, ΔTWT record indicates (i) that the ITF was weaker during MIS 6 and MIS
627 2-4 compared to the late Holocene, and was enhanced during MIS8, MIS 7, MIS 5 and the
628 early Holocene, and that (ii) it varied with a strong precession-related component. We
629 conclude that this precession component results from the direct link between ITF strength and

SE monsoon wind intensity, driven by boreal summer insolation. Today, the ITF is strongest during the SE monsoon season and our results suggest therefore that this seasonal pattern is also what could explain the ITF variability at the orbital timescale. On glacial-interglacial timescale, sea level changes may exert an effect on the TWT changes at site MD98-2165 by shallowing the ITF pathways although it fails to explain all the observations. An alternative explanation rests upon past changes in the intensity of the Great Conveyor Belt, which may have driven the glacial-interglacial ITF change. Further studies are needed to disentangle underlying mechanisms driving the glacial-interglacial ITF changes.

Acknowledgments

This research is founded by INSU/LEFE MAGICS project. X. Pang acknowledges financial support from the China Scholarship Council. We thank editor Antje Voelker and three anonymous reviewers for their constructive comments.

Data availability

The dataset generated for this study are available at www.pangaea.de.

References:

Anand, P., Elderfield, H., Conte, M., 2003. Calibration of Mg/Ca thermometry in planktonic foraminifera from a sediment trap time series. Paleoceanography 18. https://doi.org/10.1029/2002kpa000846

Barker, S., Greaves, M., Elderfield, H., 2003. A study of cleaning procedures used for foraminiferal Mg/Ca paleothermometry. Geochem Geophys Geosystems 4, n/a-n/a. https://doi.org/10.1029/2003GC000559

Beal, L.M., De Ruijter, W.P.M., Biastoch, A., Zahn, R., SCOR/WCRP/IAPSO Working Group 136, Cronin, M., Hermes, J., Lutjeharms, J., Quartly, G., Tozuka, T., Baker-Yeboah, S., Bornman, T., Cipollini, P., Dijkstra, H., Hall, I., Park, W., Peeters, F., Penven, P., Ridderinkhof, H., Zinke, J., 2011. On the role of the Agulhas system in ocean circulation and climate. Nature 472, 429–436. https://doi.org/10.1038/nature09983

Blaauw, M., Christen, J.A., others, 2011. Flexible paleoclimate age-depth models using an autoregressive gamma process. Bayesian analysis 6, 457–474.

Bolliet, T., Holbourn, A., Kuhnt, W., Laj, C., 2011. Mindanao Dome variability over the last 160 kyr: Episodic glacial cooling of the West Pacific Warm Pool. …. https://doi.org/10.1029/2010PA001966

Carton, J., Giese, B., 2008. A reanalysis of ocean climate using Simple Ocean Data Assimilation (SODA). Monthly Weather Review. https://doi.org/10.1175/2007MWR1978.1

Dang, H., Jian, Z., Bassinot, F., Qiao, P., Cheng, X., 2012. Decoupled Holocene variability in surface and thermocline water temperatures of the Indo-Pacific Warm Pool. Geophysical Research Letters 39.

DiNezio, P.N., Tierney, J.E., Otto-Bliesner, B.L., Timmermann, A., Bhattacharya, T., Rosenbloom, N., Brady, E., 2018. Glacial changes in tropical climate amplified by the Indian Ocean. Science advances 4, eaat9658.

Fan, W., Jian, Z., Chu, Z., Dang, H., Wang, Y., Bassinot, F., Han, X., Bian, Y., 2018. Variability of the Indonesian Throughflow in the Makassar Strait over the Last 30 ka. Scientific Reports 8. https://doi.org/10.1038/s41598-018-24055-1

Gordon, A., 2005. The Indonesian Seas. Oceanography, 18(4), 14.

Hammer, Ø., Harper, D.A., Ryan, P.D., others, 2001. PAST: Paleontological statistics software package for education and data analysis. Palaeontologia electronica 4, 9.

Heaton, T.J., Köhler, P., Butzin, M., Bard, E., Reimer, R.W., Austin, W.E.N., Ramsey, C.B., Grootes, P.M., Hughen, K.A., Kromer, B., Reimer, P.J., Adkins, J., Burke, A., Cook, M.S., Olsen, J., Skinner, L.C., 2020. Marine20—The Marine Radiocarbon Age Calibration Curve (0–55,000 cal BP). Radiocarbon 62, 779–820. https://doi.org/10.1017/RDC.2020.68

Holbourn, A., Kuhnt, W., Xu, J., 2011. Indonesian Throughflow variability during the last 140 ka: the Timor Sea outflow. Geological Society 355, 283–303. https://doi.org/10.1144/SP355.14

Hu, S., Zhang, Y., Feng, M., Du, Y., Sprintall, J., Wang, F., Hu, D., Xie, Q., Chai, F., 2019. Interannual to Decadal Variability of Upper-Ocean Salinity in the Southern Indian Ocean and the Role of the Indonesian Throughflow. J. Climate 32, 6403–6421. https://doi.org/10.1175/JCLI-D-19-0056.1

Kuswardani, R.T.D., Qiao, F., 2014. Influence of the Indonesian Throughflow on the upwelling off the east coast of South Java. Chinese science bulletin 59, 4516–4523.

Laskar, J., Robutel, P., Joutel, F., Gastineau, M., Correia, A., Levrard, B., 2004. A long-term numerical solution for the insolation quantities of the Earth. Astronomy & Astrophysics 428. https://doi.org/10.1051/0004-6361

Lee, S.-K., Park, W., Baringer, M.O., Gordon, A.L., Huber, B., Liu, Y., 2015. Pacific origin of the abrupt increase in Indian Ocean heat content during the warming hiatus. Nature Geoscience 8, 445–449. https://doi.org/10.1038/ngeo2438

Levi, C., 2003. Étude des variations climatiques de la zone Indo-Pacific: Rôle des basses altitudes dans la variabilité millénaire du climat. Univ. of Paris 11, Orsay, France.

Levi, C., Labeyrie, L., Bassinot, F., Guichard, F., Cortijo, E., Waelbroeck, C., Caillon, N., Duprat, J., Thibault, de G.-T., Elderfield, H., 2007. Low-latitude hydrological cycle and rapid climate changes during the last deglaciation. Geochemistry Geophysics Geosystems 8. https://doi.org/10.1029/2006gc001514

Lin, L., Khider, D., Lisiecki, L.E., Lawrence, C.E., 2014. Probabilistic sequence alignment of stratigraphic records. Paleoceanography 29, 976–989. https://doi.org/10.1002/2014PA002713

Linsley, B., Rosenthal, Y., Oppo, D., 2010. Holocene evolution of the Indonesian throughflow and the western Pacific warm pool. Nature Geoscience 3, 578–583. https://doi.org/10.1038/ngeo920

Lisiecki, L., Raymo, M., 2005. A Pliocene-Pleistocene stack of 57 globally distributed benthic delta O-18 records. Paleoceanography 20. https://doi.org/10.1029/2004pa001071

Lisiecki, L., Stern, J., 2016. Regional and global benthic δ18O stacks for the last glacial cycle. Paleoceanography 31, 1368–1394. https://doi.org/10.1002/2016PA003002

Locarnini, R.A., Mishonov, A.V., Antonov, J.I., Boyer, T.P., Garcia, H.E., Baranova, O.K., Zweng, M.M., Paver, C.R., Reagan, J.R., Johnson, D.R., others, 2013. World ocean atlas 2013. Volume 1, Temperature.

Lückge, A., Mohtadi, M., Rühlemann, C., Scheeder, G., Vink, A., Reinhardt, L., Wiedicke, M., 2009. Monsoon versus ocean circulation controls on paleoenvironmental conditions off southern Sumatra during the past 300,000 years. Paleoceanography 24.

Mohtadi, M., Steinke, S., Groeneveld, J., Fink, H.G., Rixen, T., Hebbeln, D., Donner, B., Herunadi, B., 2009. Low-latitude control on seasonal and interannual changes in planktonic foraminiferal flux and shell geochemistry off south Java: A sediment trap study. Paleoceanography 24. https://doi.org/10.1029/2008pa001636

Mohtadi, M., Oppo, D.W., Steinke, S., Stuut, J.-B.W., Ricardo, P.-H., Hebbeln, D., Lueckge, A., 2011a. Glacial to Holocene swings of the Australian-Indonesian monsoon. Nature Geoscience 4. https://doi.org/10.1038/ngeo1209

Mohtadi, M., Oppo, D., Lückge, A., Ricardo, D.-H., Steinke, S., Groeneveld, J., Hemme, N., Hebbeln, D., 2011b. Reconstructing the thermal structure of the upper ocean: Insights from planktic foraminifera shell chemistry and alkenones in modern sediments of the tropical eastern Indian Ocean. Paleoceanography 26, n/a-n/a. https://doi.org/10.1029/2011PA002132

Peeters, F., Acheson, R., Brummer, G., de Ruijter, W., Schneider, R., Ganssen, G., Ufkes, E., Kroon, D., 2004. Vigorous exchange between the Indian and Atlantic oceans at the end of the past five glacial periods. Nature 430, 661–665. https://doi.org/10.1038/nature02785

Paillard, D., Labeyrie, L., Yiou, P., 1996. Macintosh program performs time-series analysis. Eos, Transactions American Geophysical Union 77, 379–379.

Pang, X., Bassinot, F., Sepulcre, S., 2020. Cleaning method impact on the Mg/Ca of three planktonic foraminifer species: A downcore study along a depth transect. Chemical Geology 549, 119690. https://doi.org/10.1016/j.chemgeo.2020.119690

Reimer, P.J., Bard, E., Bayliss, A., Beck, J.W., Blackwell, P.G., Ramsey, C.B., Buck, C.E., Cheng, H., Edwards, R.L., Friedrich, M., Grootes, P.M., Guilderson, T.P., Haflidason, H., Hajdas, I., Hatté, C., Heaton, T.J., Hoffmann, D.L., Hogg, A.G., Hughen, K.A., Kaiser, K.F., Kromer, B., Manning, S.W., Niu, M., Reimer, R.W., Richards, D.A., Scott, E.M., Southon, J.R., Staff, R.A., Turney, C.S.M., van der Plicht, J., 2013. IntCal13 and Marine13 Radiocarbon Age Calibration Curves 0–50,000 Years cal BP. Radiocarbon 55, 1869–1887. https://doi.org/10.2458/azu_js_rc.55.16947

Rosenthal, Y., S, P.-C., Lear, C., Bard, E., Barker, S., Billups, K., Bryan, M., Delaney, M., PB, deMenocal, Dwyer, G., Elderfield, H., German, C., Greaves, M., Lea, D., Marchitto, T., Pak, D., Paradis, G., Russell, A., Schneider, R., Scheiderich, K., Stott, L., Tachikawa, K., Tappa, E., Thunell, R., Wara, M., Weldeab, S., Wilson, P., 2004. Interlaboratory comparison study of Mg/Ca and Sr/Ca measurements in planktonic foraminifera for paleoceanographic research. Geochemistry Geophysics Geosystems 5, n/a-n/a. https://doi.org/10.1029/2003gc000650

Southon, J., Kashgarian, M., Fontugne, M., Metivier, B., Yim, W.W.-S., 2002. Marine Reservoir Corrections for the Indian Ocean and Southeast Asia. Radiocarbon 44, 167–180. https://doi.org/10.1017/S0033822200064778

Sprintall, J., Révelard, A., 2014. The Indonesian Throughflow response to Indo-Pacific climate variability. Journal of Geophysical Research: Oceans 119, 1161–1175. https://doi.org/10.1002/2013JC009533

Sprintall, J., Wijffels, S., Molcard, R., Jaya, I., 2009. Direct estimates of the Indonesian Throughflow entering the Indian Ocean: 2004-2006. Journal of Geophysical Research-Oceans 114, 19. https://doi.org/10.1029/2008jc005257

Steinke, S., Prange, M., Feist, C., Groeneveld, J., Mohtadi, M., 2014. Upwelling variability off southern Indonesia over the past two millennia. Geophysical Research Letters 41, 7684–7693. https://doi.org/10.1002/2014GL061450

Susanto, R.D., Gordon, A.L., Zheng, Q., 2001. Upwelling along the coasts of Java and Sumatra and its relation to ENSO. Geophysical Research Letters 28, 1599–1602. https://doi.org/10.1029/2000GL011844

Szeremeta, N., Bassinot, F., Balut, Y., Labeyrie, L., Pagel, M., 2004. Oversampling of sedimentary series collected by giant piston corer: Evidence and corrections based on 3.5-kHz chirp profiles. Paleoceanography 19. https://doi.org/10.1029/2002pa000795

Talley, L., 2013. Closure of the Global Overturning Circulation Through the Indian, Pacific, and Southern Oceans: Schematics and Transports. Oceanography 26, 80–97. https://doi.org/10.5670/oceanog.2013.07

Waelbroeck, C., Labeyrie, L., Michel, E., Duplessy, J., JF, M., Lambeck, K., Balbon, E., Labracherie, M., 2002. Sea-level and deep water temperature changes derived from benthic foraminifera isotopic records. Quaternary Science Reviews 21, 295–305. https://doi.org/10.1016/s0277-3791(01)00101-9

Waelbroeck, C., Levi, C., Duplessy, J., Labeyrie, L., Michel, E., Cortijo, E., Bassinot, F., Guichard, F., 2006. Distant origin of circulation changes in the Indian Ocean during the last deglaciation. Earth and Planetary Science Letters 243, 244–251. https://doi.org/10.1016/j.epsl.2005.12.031

Wang, X., Jian, Z., Lückge, A., Wang, Y., Dang, H., Mohtadi, M., 2018. Precession-paced thermocline water temperature changes in response to upwelling conditions off southern Sumatra over the past 300,000 years. Quaternary Science Reviews 192, 123–134. https://doi.org/10.1016/j.quascirev.2018.05.035

Xu, J., Holbourn, A., Kuhnt, W., Jian, Z., Kawamura, H., 2008. Changes in the thermocline structure of the Indonesian outflow during Terminations I and II. Earth and Planetary Science Letters 273, 152–162. https://doi.org/10.1016/j.epsl.2008.06.029

Xu, J., Kuhnt, W., Holbourn, A., Regenberg, M., Andersen, N., 2010. Indo-Pacific Warm Pool variability during the Holocene and Last Glacial Maximum. Paleoceanography 25, n/a-n/a. https://doi.org/10.1029/2010pa001934

Zuraida, R., Holbourn, A., Nuernberg, D., Kuhnt, W., Duerkop, A., Erichsen, A., 2009. Evidence for Indonesian Throughflow slowdown during Heinrich events 3-5. Paleoceanography 24. https://doi.org/10.1029/2008pa001653